Int. J. Electrochem. Sci., 8 **(2013)** 8812 - 8822

International Journal of
ELECTROCHEMICAL
SCIENCE
www.electrochemsci.org

Corrosion Behavior of Alloy 800 in Simulated Crevice Solutions

Huihui Wang[1, 2], *Jihui Wang*[1, 2,*], *Congwei Fu*[2], *Ke Wang*[2]

[1] State Key Laboratory of Hyraulic Engineering Simulation and Safety, Tianjin University, Tianjin 300072, R R China
[2] Tianjin Key Laboratory of Composite and Functional Materials, School of Materials Science and Engineering, Tianjin University, Tianjin 300072, P R China
[*]E-mail: jhwang@tju.edu.cn

Received: 5 January 2013 / *Accepted:* 24 April 2013 / *Published:* 1 June 2013

Corrosion behavior of alloy 800 in simulated steam generator crevice solutions was investigated by using potentiodynamic polarization, cyclic voltammetry, cyclic polarization techniques together with scanning electron microscopy and energy dispersive spectroscopy. The experimental results revealed that the passive range and pitting corrosion potential of alloy 800 in the solution containing both thiosulphate and chloride ions are lower than that in the solution with $S_2O_3^{2-}$ or Cl^- ion alonely or the combination of SO_4^{2-} and Cl^- ions, but the passive current density of alloy 800 in thiosulphate and chloride containing solution is the largest among the five simulated solutions. The passive film of alloy 800 in simulated crevice solution is mainly iron oxides and Cr_2O_3. The addition of Cl^- and $S_2O_3^{2-}$ ions in the solution could hinder the formation of passive film on alloy 800, and thus alloy 800 has a higher pitting corrosion susceptibility. Finally the pitting mechanism of alloy 800 in $S_2O_3^{2-}$ and Cl^- containing solution was discussed.

Keywords: Alloy 800, thiosulphate, localized corrosion, pitting corrosion susceptibility

2. INTRODUCTION

Alloy 800 is a kind of steam generator (SG) tube materials which preferentially used in CANDU™ reactors and some pressurized water reactor (PWR) systems. Degradation of alloy 800 SG tubing has only been found in a few tubes at a limited number of stations despite the large number of SG tube operated years accumulated to date. In the SG feedwater, sulphate is one of the major impurities, which can be reduced to intermediate oxidation state sulphur (IOSS) under the assistance of hydrazine. Among the identified possible IOSS species, thiosulphate is the most possible species which could cause pitting corrosion [1], intergranular attacks and stress corrosion cracking (SCC) of alloy 800 [2-4].

Fang and Staehle investigated the surface characteristics of alloys 600, 690 and 800 after polarization, and found that the intergranular corrosion was occurred mainly in solutions containing SO_4^{2-}, sulfite (SO_3^{2-}), tetrathionate ($S_4O_6^{2-}$) and $S_2O_3^{2-}$ [5]. Zhu and Luo [6] found that the corrosion susceptibility of alloy 800 in thiosulfate-contained chemistries could be accelerated with localized microstructure deformation which caused by both tensile stress and compression stress. Wang and Smialowska [8] suggested the pit initiation of alloy 600 in the thiosulphate containing solution at potentials lower than those necessary to initiate pits in pure chloride solution was resulted by the reaction of $Ni_3S_2 + 8H_2O = 3Ni^{2+} + 2HSO_4^- + 14H^+ + 18e^-$. Ho and Yu [7] also proved that thiosulfate plays an important role in the growth process of corrosion pit by reacting with nickel ions on the surface of inconel 600. It has been suggested that the reduction of metastable thiosulphate ion to a lower oxidation state, such as elemental sulphur and sulphide, at the localized corrosion site was responsible for the pitting or crevice corrosion of stainless steel in chloride solution [9].

Meanwhile, it was also found that thiosulphate ions could promote the localized corrosion of stainless steel in chloride solution [1]. Meguid and Mahmoud [10] studied the effect of different sulphur containing anions added to chloride on pitting corrosion of 304SS, and found that 10^{-2} mol/L $Na_2S_2O_3$ or 0.1 mol/L NaCl strongly reduced the pitting induction time than that recorded in 0.1 mol/L NaCl, whereas other sulphur species had a little effect on the value. In sodium chloride solution, the addition of sodium thiosulfate could enhance the pitting corrosion [11]. Laitinen [12] revealed that in the presence of thiosulfate a non-protective film formed on 304 stainless steel, or thiosulfate hindered the form action of a passive film on 304 stainless steel.

In order to minimize the corrosion failure of alloy 800, it is important to understand the corrosion behavior of alloy 800 in simulated crevice chemistry. The projective of this paper is to investigate the passivation degradation and local pitting behavior of alloy 800 in simulated crevice chemistry by using electrochemical techniques and surface analysis methods, and then the corrosion mechanism of alloy 800 in $S_2O_3^{2-}$ and Cl^- solution was discussed.

2. EXPERIMENTAL

2.1. Material and test solutions

Alloy 800 tubing with dimensions of 1.13 mm nominal wall thickness and 15.88 mm outside diameter was used, whose composition was shown in Table 1. All samples were connected electronically to copper wire and sealed in epoxy. Before testing, the exposed surface was mechanically polished with wet silicon carbide papers in the sequence of 400, 800, 1000, 1500, 2000 grit, rinsed copiously with deionized water, and then dried in desiccator for 24h.

Analytical chemical reagents and deionized water were used to prepare the test solutions according to Table 2, in which R1 and R2 were used as reference solutions.

Table 1. Chemical composition of alloy 800 (wt%)

C	Si	Mn	P	S	Cr	Ni	Co	Ti	Cu	Al	N	Fe
0.017	0.46	0.5	0.012	0.001	21.87	32.78	0.01	0.48	0.02	0.29	0.016	43.2

Table 2. Simulated CANDU SG neutral crevice chemistry ($mol \cdot L^{-1}$)

Solution	NaCl	KCl	$CaCl_2$	SiO_2	Na_2SO_4	$Na_2S_2O_3$
R1	0	0	0	0	0.15	0
R2	0	0	0	0	0	0.075
NC-0	0.30	0.05	0.15	0.05	0	0
NC-1	0.30	0.05	0.15	0.05	0.15	0
NC-2	0.30	0.05	0.15	0.05	0	0.075

2.2 Electrochemical measurement

All the electrochemical measurements of alloy 800 were carried out by VersaSTAT 4 electrochemical workstation (Princeton Applied reseach, USA) and VersaStudio control software. The electrolytic cell consisted of a traditional three electrodes system. Alloy 800 with an area of 3.118 cm^2 were used as the working electrode (WE). A saturated calomel electrode (SCE) connected with a Luggin capillary was used as reference electrode (RE), and a platinum electrode was used as counter electrode (CE). Before the electrochemical measurement, all the samples were cathodicly polarised at −1.0 V_{SCE} for 10 min in order to reduce the air-formed oxide film on the alloy surface. And then the specimens were exposed at open-circuit for 30 min before starting the experiments. All tests were performed at ambient temperature in aerated state.

2.2.1Potentiodynamic polarization

Potentiodynamic polarizations of alloy 800 were performed by sweeping the potential in the positive direction at a certain potential scan rate of 0.1667mV/s until a destination potential was reached.

2.2.2 Cyclic voltammetry (CV)

CV technique was performed by sweeping potential from -0.6V to the maximum value of passive region according polarization curves in each solution and then in the reverse direction back to the initial value at a relatively high potential scan rate (50 mV/s).The measured current–potential curves were used to analyze the general electrochemical behavior of the alloy.

2.2.3 Cyclic Polarization (CP)

Cyclic polarization technique was used to determine the susceptibility of alloy 800 to pitting corrosion. Pitting potential (E_{pit}) and protection potential (E_{prot}) were measured to characterize the pitting susceptibility. E_{pit} denoted the potential at which pits initiated during the forward scan and the current increased abruptly. E_{prot} was the potential at which the pits were repassivated during the reverse scan, which was measured by the point of intersection of forward scan curve and reverse scan curve.

During the test, the potential was firstly scanned potentiodynamically at a rate of 1 mV/s from -50 mV to a potential corresponding to a current density of 10mA/cm^2, and then the scan direction was reversed. The reversed scan was continued until the protection potential was identified.

2.3 Surface characterization

After cyclic polarization，the surface morphology and composition of corroded alloy 800 were observed and determined by a field-emission scanning electron microscopy (FE-SEM S4800; Hitachi, Japan) and an energy dispersive X-ray analyzer (EDAX Genesis, Hitachi, Japan).

3. RESULTS AND DISCUSSION

3.1 Polarization curve

Figure 1 is the potentiodynamic polarization curves of alloy 800 in the simulated SG crevice solution. It was seen that there is a wide passivition region from -50 to about 1000 mV for alloy 800 in solutions of R1 and R2. In solutions of NC-0 and NC-1, the passivition region of alloy 800 is located between -100 mV to 600 mV, and there are some current fluctuations which indicated the occurrence of metastable pitting owing to the presence of chlorid ion. But in NC-2 solution, alloy 800 shows a minimum passivition region from -200 to 0 mV, and the passivating current density is about 10^{-6} A/cm^2 which is one order of magnitude larger than those of in other four solutions. This higher current density is possibly due to the fact that $S_2O_3^{2-}$ enhances the anodic dissolution of alloying elements into the solution. This implies that thiosulfate has a strong effect on the corrosion behaviour of alloy 800 and may cause the degradation of oxide film on alloy 800.

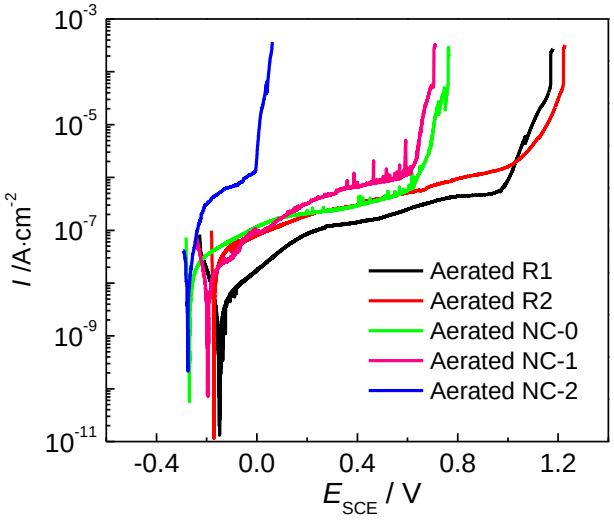

Figure 1 Potentiodynamic polarization curves of alloy 800 in the five simulated crevice solutions

3.2 Cyclic voltammetry curve

Fig. 2 shows the cyclic voltammograms of alloy 800 in the five simulated crevice solutions. Anodic peak A1 located at about -0.5V and its cathodic counterpart C1 occur in all the five solutions. Peak A2 and cathodic counterpart C2 occur in the solution of R1, R2, NC-0, NC-1 (Fig.2a-2d) and is absent in NC-2 solution (Fig.2e). The current density within the potential range from -0.25 to 0.25 V_{SCE} decreased with the increasing of scanning times due to the existence of oxides formed in the first scan.

Since Fe, Ni and Cr are the dominated elements in alloy 800, the reactions involving Fe, Ni and Cr are of primary consideration in interpreting the cyclic voltammogram. A1 indicates the oxidation of Fe(0) to Fe(II)[13], which reflects the initiation of passivity. The broad peak A2 reflects the oxidation of Fe(II) to Fe_3O_4 or Fe_2O_3 and Cr to Cr_2O_3[14], which has already been present on the surface but not completely reduced after the cathodic pretreatment at -1.0V. During the following anodic scans, A2 shifts positively due to the oxidation of $Cr_2O_3 \rightarrow CrO_4^{2-}$[15].The charge involved in peak Cl appears larger than that of A1, and proved that FeO is completely reduced and that is why the current density keeps the same at potential -0.5V during the following scanning.

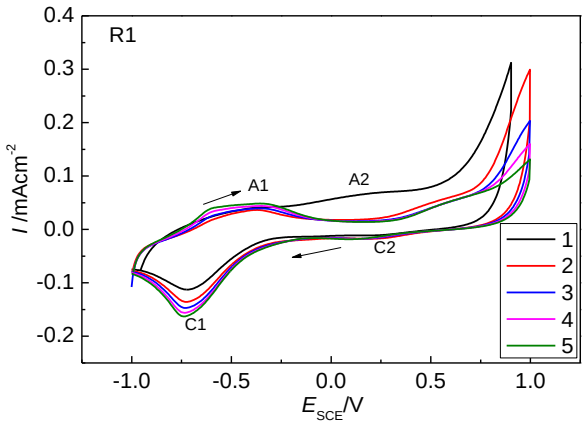

(a) R1solution

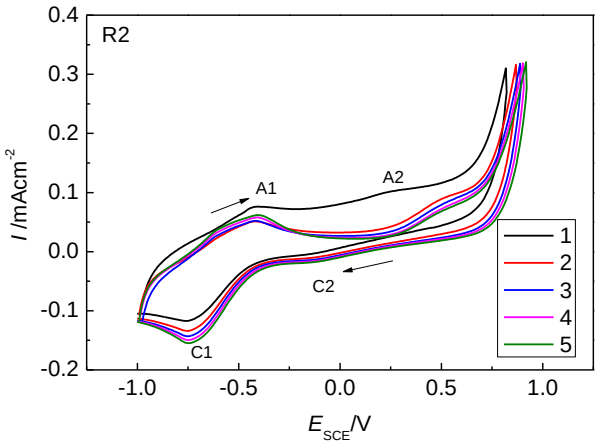

(b) R2 solution

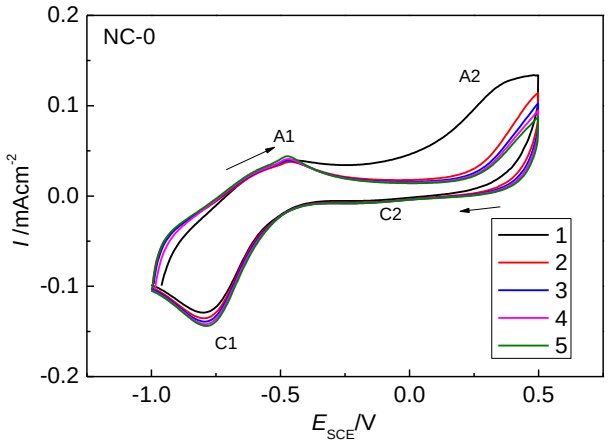

(c) NC-0 solution

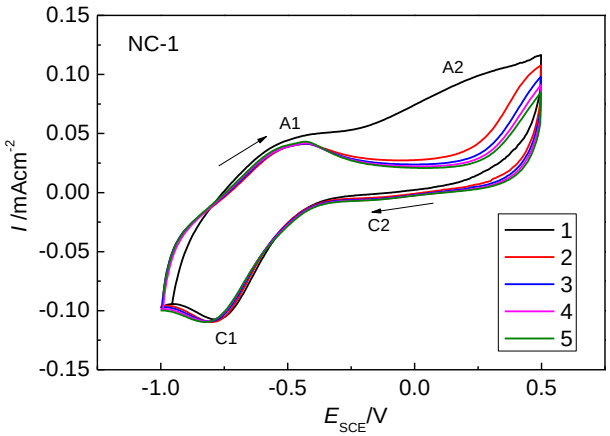

(d) NC-1solution

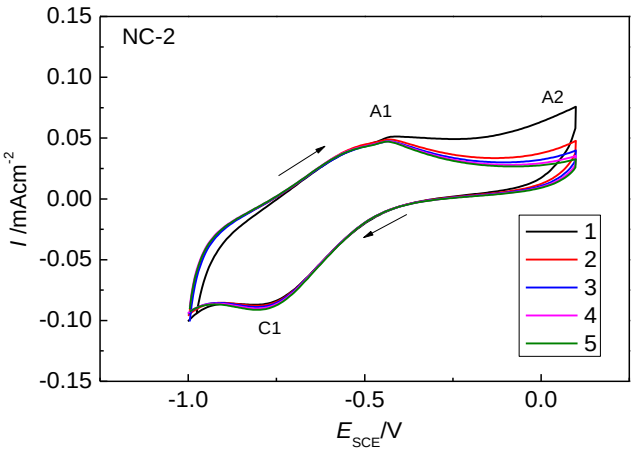

(e) NC-2 solution

Figure 2. Cyclic voltammograms of alloy 800 in the five simulated crevice solutions, in which number 1-5 represent the times of scanning cycle, A1 to A3 represent the anodic peaks, C1 to C2 represent the cathodic peaks corresponded with A1to A3.

The small cathodic peak C2 which is the conjugate of anodic peak A2 manifests the defective Cr_2O_3 barrier layer on the surface, and is difficult to reduce. The abrupt increase of current at potential larger than 50mV in Fig.2e is probably due to the transpassive dissolution (presumably $Cr_2O_3 \rightarrow CrO_4^{2-}$). Dutta [16] revealed by X-ray photoelectron spectroscopy that the surface film formed on the alloy 800 at the onset of passivity consisted of Cr^{3+} (as Cr_2O_3), without any Fe^{3+}/Fe^{2+} or Ni^{2+}. The possible reasons for the significant enrichment of Cr within the barrier film are the preferential oxidation of Cr prior to the onset of Fe oxidation [17], and chromium cations haves a lower mobility than iron cations [14,18].

3.3 Cyclic polarization curve

The cyclic polarization curves of alloy 800 in NC-0, NC-1 and NC-2 solutions are shown in Fig.3. It was seen that that the corrosion potential and passive current density of alloy 800 in NC-0, NC-1 and NC-2 solutions are almost the same. However, the pitting potential and repassivation potentials in NC-2 solution are found as 0.180 V and -0.120V respectively, which are lower than those in NC-0 and NC-1 solutions. This phenomenon may implies that $S_2O_3^{2-}$ had a detrimental effect on the stability of oxide film on alloy 800, or thiosulfate hinders the formation of a passive film or forms a very weak surface film on alloy 800. Similar behavior was reported for 310 SS in ammonium chloride solution with sodium thiosulfate addition, in which that the presence of sodium thiosulfate enhanced the pitting corrosion as indicated by the decrease in pitting potential[11].

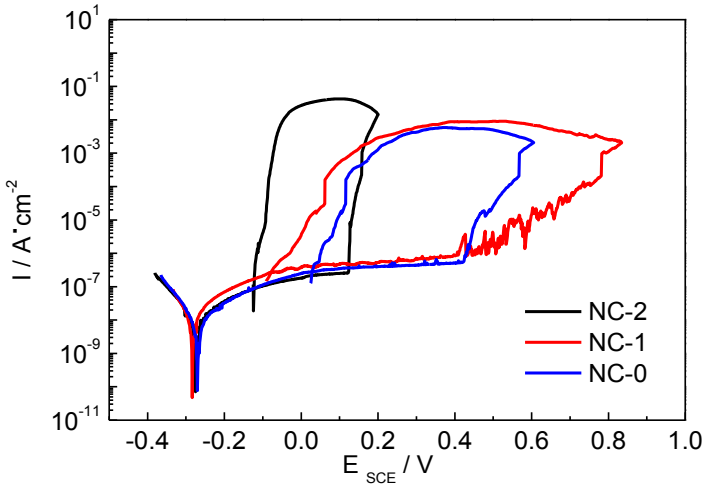

Figure 3 Cyclic polarization curves of alloy 800 in NC-0, NC-1 and NC-2 solutions

3.4 Surface morphology

Fig.4 shows the surface morphology of alloy 800 after cyclic polarization in NC-0, NC-1 and NC-2 solutions. Few corrosion pits were formed on the surface of alloy 800 in NC-0 and NC-1 solutions, whereas much more corrosion pits were found on alloy 800 in NC-2 solution.

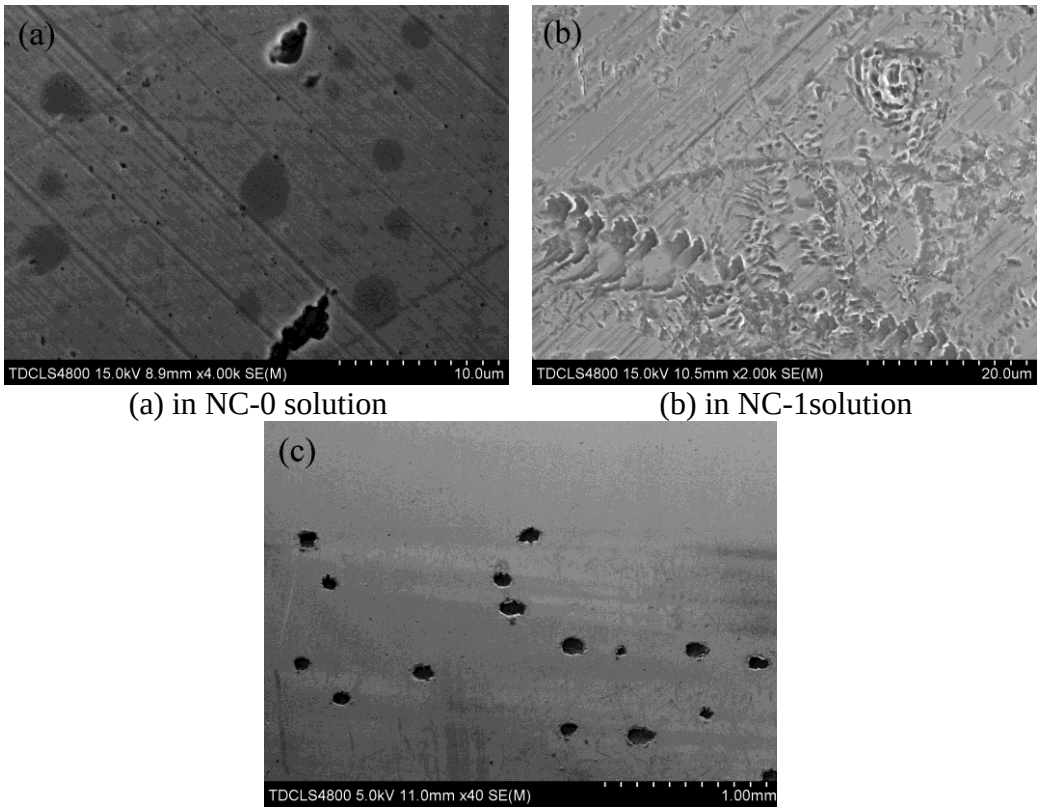

(a) in NC-0 solution (b) in NC-1solution

(c) in NC-2 solution

Figure 4. Surface morphology of alloy 800 after cyclic polarization in (a) NC-0, (b) NC-1 and (c) NC-2 solutions

The surface morphology and element distribution around corrosion pit of alloy 800 after cyclic polarization in NC-2 solution are shown in Fig.5. It could be observed that significant sulphur is found in the bottom of corrosion pit while sulphur is hardly detected on the alloy surface, which indicating that $S_2O_3^{2-}$ reduction reaction took part in corrosion process. According the point defect model[19, 20], the chloride ion was absorbed into oxygen vacancies at the barrier/outer layer interface, increased the local cation vacancy concentration and then increased the electro migration-dominated flux of cation vacancies from the barrier layer/outer layer interface to the metal/barrier interface. When arrived at the metal/barrier layer interface, cation vacancies are annihilated by an oxidative injection of cation from the metal into the film. However, if the rate of annihilation cannot accommodate the enhanced flux of cation vacancies, the accumulation of cation vacancies with the acritical concentration occurs at the interface metal/oxide and causes the collapse of the film. The collapse sites in the alloy film dissolve with a higher rate, and the sulphur ions accumulated inside the big pits via the following possible reactions[21]

$$S_2O_3^{2-}+6H^++4e^- = 2S+ 3H_2O \quad (1)$$

$$S+2H^++2e^- = H_2S_{aq} \quad (2)$$

$$(n/2)H_2S_{aq}+M^{n+} = MS_{n/2}+nH^+ \quad (3)$$

Where M^{n+} are Fe, Ni or Cr ions which are produced by chloride pitting. The addition of thiosulphate ions could further enhance the anodic dissolution behavior and impede the repassivation of alloy 800. So the combination of $S_2O_3^{2-}$ and chloride in the solution have a synergistic effect on the

pitting corrosion of alloy 800. The comparison between the EDAX map Fe, Ni and Cr elements implied that the dissolution of Fe was the highest, which was probably promoted by the presence of sulphide in the test solution. It was also possible that the metal oxide reacted with the reduced sulfur to form sulphide, and thus degraded the passive film.

It was also seen that titanium element was also found in the corrosion pit, which consisted with Dutta's results [16]. The formation of primary titanium nitride and carbonitride particles in Cr-Ni-Fe based alloy could not be avoided during the solidification process. And these intermetallic phases may act as the active sites to destroy the integrality of passive film and initiate the corrosion pit.

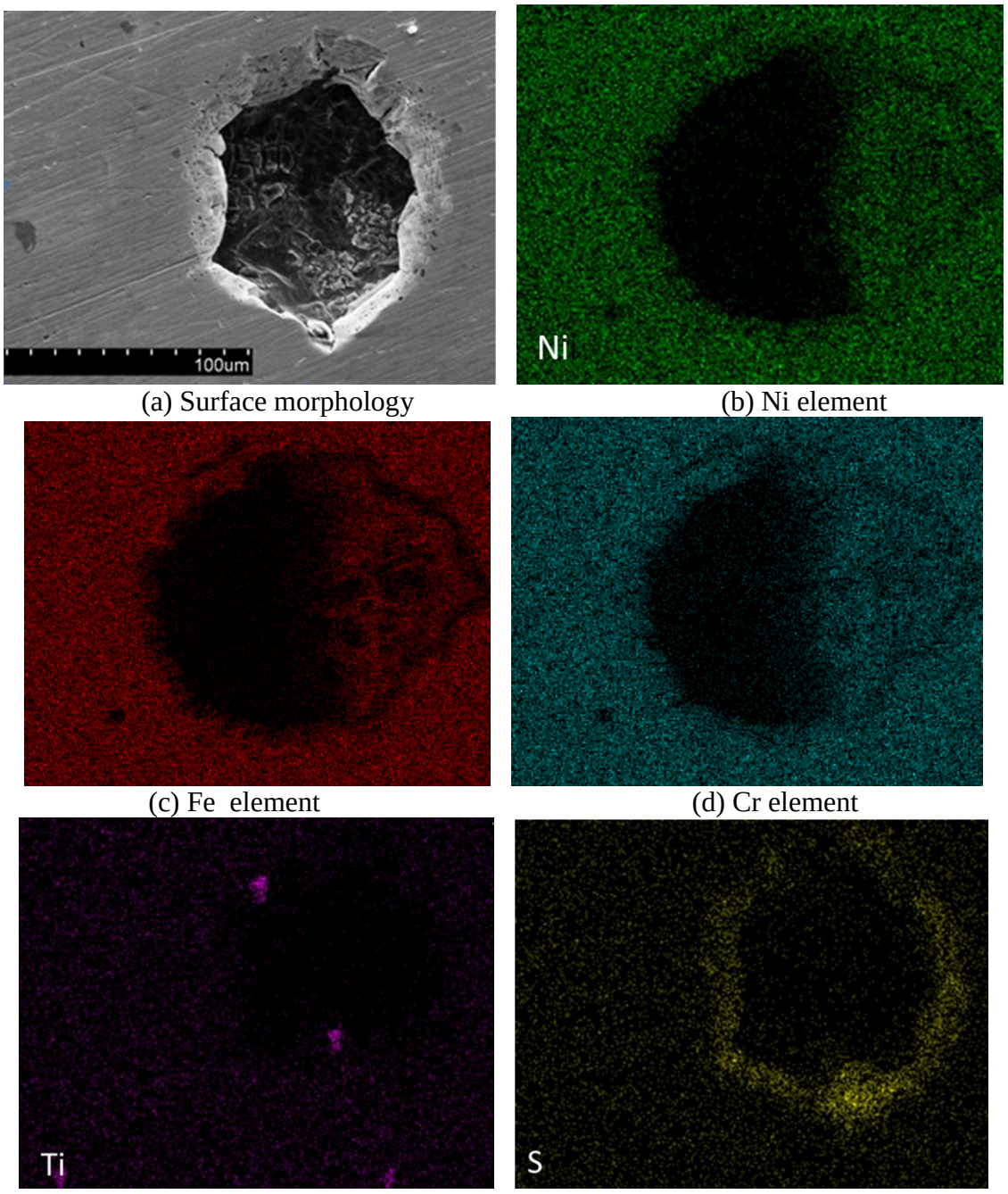

(a) Surface morphology (b) Ni element

(c) Fe element (d) Cr element

(e) Ti element (f) S element

Figure 5. Surface morphology and element distribution around corrosion pit of alloy 800 after cyclic polarization in NC-2 solution

4. CONCLUSION

Based on the previous published papers [22-27], the conclusions are drawn:

(1) The passive range and pitting corrosion potential of alloy 800 in the solution containing both thiosulphate and chloride ions are lower than that in the solution with $S_2O_3^{2-}$ or Cl^- ion alonely or the combination of SO_4^{2-} and Cl^- ions, whereas the passive current density of alloy 800 in thiosulphate and chloride containing solution is the largest among the five simulated solutions.

(2) The passive film of alloy 800 in simulated crevice solution is mainly iron oxides and Cr_2O_3. The addition of Cl^- and $S_2O_3^{2-}$ ions in the solution could hinder the formation of passive film on alloy 800, and thus alloy 800 has a higher pitting corrosion susceptibility.

ACKNOWLEDGEMENTS
This paper is financially supported by National Key Basic Research Program of China (2011CB610505) and Specialized Research Fund for the Doctoral Program of Higher Education (20120032110029).

References

1. W. Tatsai, Z. H. lee, J. T. Lee, M. C. Tsai, P. Holo, *Mater. Sci. Eng.* A, 118 (1989) 121-129.
2. W. Yang, Z. Lu, D. Huang, D. Kong, G. Zhao, J. Congleton, *Corros. Sci.*, 43 (2001) 963-977.
3. S.S. Hus, S.C. Tsai, J. J. Kai , C.H. Tsai, *J. Nuclear Mater*., 184 (1991) 97-106.
4. M. Gomez-Duran, D. D. Macdonald, *Corros. Sci.*, 45 (2003) 1455-1471.
5. Z. Fang, R.W. Staehle, Corrosion, 55 (1999) 355-379.
6. R. K. Zhu, J. L. Luo, *Electrochem. Commun*., 12 (2010) 1752-1755.
7. J.T. Ho, G.P. Yu, *Corrosion*, 48 (1992) 147-158.
8. W. T. Tsai, Z. H. Lee, J. T. Lee, M. C. Tsai, H. Ping, *Mater. Sci. Eng.* A, 118 (1989) 121-129.
9. R. C. Newman, H. S. Isaacs, B. Alman, *Corrosion*, 38 (1982) 261-265.
10. E. A. Abd El Meguid, N. A. Mahmoud, S. S. AbdElRehim, *Mater. Chem. Phys*., 63 (2000) 67-74.
11. H. S. Kuo, H. Chang. W. T. Tsai, *Corros. Sci*., 41 (1999) 669-684.
12. T. Laitinen, *Corros. Sci*., 42 (2000) 421-441.
13. E. M. A. Martini, I. L. Muller, *Corros. Sci*., 42 (2000) 443-454.
14. Y. Zhang, M. Urquidi-Macdonald, G. R. Engelhardt, D. D. Macdonald, *Electrochim. Acta*, 69 (2012) 1-11.
15. T. Piao, S. M. Park, *J. Electrochem. Soc*., 144 (1997) 3371-3377.
16. R. S. Dutta, R. Purandare, A. Lobo, S. K. Kulkarni, G. K. Dey, *Corros. Sci*., 46 (2004) 2937-2953.
17. R. Kirchheim, B. Heine, H. Fischmeister, S. Hofmann, H. Knote, U. Stolz, *Corros. Sci*., 29 (1989) 899-917.
18. G. Lorang, M. Da Cunha Belo, A.M.P. Simões, M. G. S. Ferreira, *J. Electrochem.Soc*., 141 (1994) 3347-3356.
19. D. D. Macdonald, *J. Electrochem. Soc*, 139 (1992) 3434-3449.
20. D. Sazou, K. Saltidou, M. Pagitsas, *El ectrochim. Acta*, 76 (2012) 48-61.
21. M. G. Faichuk, S. Ramamurthy, W. M. Lau, *Corros. Sci*., 53 (2011) 1383-1393.
22. D. H. Xia, C. Zhou, Y. H. Liu, J. H. Wang, C. W. Fu, K. Wang, M. Li, *Electrochemistry*, 81(2013) 262–268.
23. C. Zhou, J. H. Wang, S. Z. Song, D. H. Xia, K. Wang, C. Shen, B. Luo, J. B. Shi, *Journal of Wuhan University of Technology-Mater. Sci. Ed.*, 28 (2013) 367-372.

24. J. B. Shi, D. H. Xia, J. H. Wang, C. Zhou, Y. H. Liu, *Trans. Tianjin Univ.*, 19 (2013) 92-97.
25. X. Zheng, D.H. Xia, H. H. Wang, C.W. Fu, *Anti-Corros. Methods Mater*. 60 (2013) accepted for publication.
26. D. H. Xia, S. Z. Song, J.H. Wang, J.B. Shi, H.C. Bi, Z. M. Gao, *Electrochem. Commun*., 15 (2012) 88-92.
27. D. H. Xia, S. Z. Song, J. H. Wang, H. C. Bi, Z. W. Han, *Acta Phys-Chim. Sin.*, 28 (2012) 121-126.